

Sub-GeV dark matter in neutron stars: halo morphologies and their suppression by vacuum-like pressure

Loreany F. Araújo,¹ Germán Lugones,² and José Ademir S. Lima¹

¹Departamento de Astronomia, Universidade de São Paulo
Rua do Matão, 1226 - 05508-900, São Paulo, SP, Brazil

²Universidade Federal do ABC, Centro de Ciências Naturais e Humanas
Avenida dos Estados 5001- Bangú, CEP 09210-580, Santo André, SP, Brazil

E-mail: loreanyfa@usp.br, german.lugones@ufabc.edu.br, jas.lima@iag.usp.br

Abstract. We investigate neutron stars that contain a unified dark sector composed of cold, degenerate fermionic dark matter and a vacuum-like dark-energy component. Within a general-relativistic two-fluid framework that allows a covariantly conserved, gradient-driven energy exchange between baryons and the dark sector, we quantify how dark microphysics reshapes global structure when the total gravitational radius need not coincide with the luminous baryonic radius. Using a state-of-the-art baryonic equation of state, we explore the halo-forming mass range for fermionic dark matter with particle masses of 400 MeV and 1 GeV, and we characterize sequences by the difference between the total and luminous radii and by the fractional difference between the total and baryonic masses. We confirm established trends: lighter fermions typically support low-density halos that increase the total radius by several kilometers at nearly fixed mass, whereas masses near 1 GeV tend to shrink halos and make the two radii appreciably closer. Our central new result is that a percent-level vacuum-like admixture markedly reduces halo formation, shrinking the radius difference from several kilometers to sub-kilometer scales and the fractional mass difference to $\lesssim 1\%$. Combined gravitational-wave and X-ray observations offer a practical route to bound the halo size and the allowed vacuum-like fraction.

Contents

1	Introduction	1
2	Dark influence on the structure equations	3
3	Results	5
3.1	Halo diagnostics from radius and mass excess	5
3.2	Mass–radius relations with luminous vs gravitational radii	9
4	Summary and conclusions	9

1 Introduction

The microscopic nature of dark matter (DM) and dark energy (DE) remains a central open problem in fundamental physics and cosmology. While a broad array of cosmological and galactic observations tightly constrains their large-scale gravitational effects, any non-gravitational couplings to the Standard Model are poorly known [1–3]. Neutron stars (NSs) provide a complementary arena to probe such interactions: their deep gravitational potentials, supranuclear densities, and long lifetimes can amplify even feeble dark couplings, yielding cumulative imprints on structure and dynamics that are, in principle, accessible to multimessenger observations.

A rich set of mechanisms has been proposed to test DM with NSs. Capture via scattering on stellar constituents can produce a bound DM population whose annihilation or kinetic heating modifies the heat budget and cooling history of otherwise cold, old NSs [4–8]. Additional possibilities include dark or baryon-number-violating decays in the interior [9], compact-object coalescences involving mirror or DM-admixed NSs with distinctive gravitational-wave signatures [10], and scenarios in which annihilation products (e.g., long-lived mediators) escape the star and generate electromagnetic or neutrino emission outside the surface, reshaping the expected multimessenger phenomenology [11–13]. Beyond thermal and high-energy messengers, dark components may also shift NS oscillation spectra (e.g., f -modes), opening a route for asteroseismology and future gravitational-wave constraints [14].

At the level of global structure, the impact of a dark component is cleanly described in a general-relativistic two-fluid framework, in which the dark and baryonic sectors possess distinct equations of state and, in general, distinct radial profiles. This viewpoint naturally organizes equilibria into compact configurations with a dark-dominated core, partially overlapping “admixed” profiles, and extended halos in which the dark density predominates outside the baryonic surface—an organizing picture already apparent in early two-fluid analyses [15–17]. Two-fluid studies with *fermionic* DM map these regimes across parameter space: sub-GeV fermions tend to support low-density halos that inflate the *gravitational* radius with comparatively small mass shifts, whereas near-GeV particles largely suppress halo formation and drive the configuration toward a baryonic baseline [18–21]. Related analyses with bosonic DM and repulsive self-interactions display analogous trends in radius and tidal response, further restricting the admissible dark fraction [22]. Crucially, when diffuse halos are present, the radius inferred from space-time observables (sensitive to the exterior metric)

does not need to coincide with the photospheric radius tied to the luminous surface; this distinction is essential for interpreting X-ray pulse profiles, self-lensing, and tidal-deformability constraints [23–25].

The last decade has delivered a qualitative leap in NS astrophysics: radio timing of massive pulsars, gravitational-wave constraints on tidal deformability from GW170817, and NICER pulse-profile inferences now anchor the equation of state (EOS) at supranuclear densities with unprecedented precision [26–30]. This multimessenger toolkit can be repurposed to test dark-sector effects. In halo-dominated configurations—where the total (gravitational) radius grows more than the mass at fixed M —the tidal deformability $\Lambda = \frac{2}{3}k_2C^{-5}$ is generically amplified, tightening GW bounds on the allowed halo extent [19, 22]. In contrast, pulse-profile modeling constrains a photospheric radius tied to the luminous surface, reinforcing the need to treat R and R_{bm} as distinct observables in any confrontation with data.

Dark-energy-like sectors can likewise influence hydrostatic balance when modeled as a vacuum-like component ($w \simeq -1$) or as part of a unified dark sector. In such cases, negative pressure can soften the effective force balance in the outer layers and reduce the radii at fixed mass, thus modifying the tidal properties and the reading of multi-messenger constraints [31]. In our previous work [31], we quantified these effects for fermionic DM with benchmark mass $m_\chi = 10$ GeV, a regime that does not produce extended halos. There we showed that introducing a vacuum-like fraction leads to a systematic contraction of the sequences and a reduction of the maximum mass, with the luminous and gravitational radii remaining closely aligned due to the absence of a diffuse dark envelope. We further demonstrated that allowing energy exchange between baryons and the dark sector via a covariantly conserved, gradient-driven source term steepens the pressure decline in the exterior layers when a vacuum-like component is present, reinforcing the net compacting trend.

The present paper is a natural continuation of that program, but focused on the *halo-forming* mass range that was not explored in [31]. Throughout, we label the sectors by the subscripts ‘bm’, ‘ χ ’, and ‘de’ for baryonic matter, DM, and DE, respectively. We move to lighter DM fermions, $m_\chi = \{400 \text{ MeV}, 1 \text{ GeV}\}$, for which two-fluid equilibria can develop low-density halos that inflate the total (gravitational) radius R relative to the luminous baryonic radius R_{bm} . For clarity, we distinguish two radii and two masses: (i) R_{bm} is the location of the baryonic surface; the associated mass M_{bm} is the gravitating mass enclosed within R_{bm} —including any DM/DE present inside—and is the quantity constrained by radiative observables from that surface; (ii) R is the outer boundary of the configuration, defined by the outermost radius at which the total pressure $p_{\text{bm}}(r) + p_\chi(r) + p_{\text{de}}(r)$ vanishes, and M is the total gravitational mass enclosed within R . We introduce data-facing diagnostics—radius and mass excesses $\Delta R \equiv R - R_{\text{bm}}$ and $\Delta M/M \equiv (M - M_{\text{bm}})/M$ —to quantify geometry-luminous decoupling across sequences, and we confront these trends with multimessenger constraints by keeping R and R_{bm} explicitly separate. Our central new result is that a *per cent level* vacuum-like admixture is sufficient to *quench* halo formation even in otherwise halo-friendly regimes, driving ΔR from multikilometer to subkilometer scales while leaving $\Delta M/M$ at the subpercent level.

The paper is organized as follows. Section 2 formulates the two-fluid stellar-structure equations with energy exchange, specifies the baryonic EOS and the fermionic DM and vacuum-like DE components, and defines the central-partition parameters used to generate sequences. Section 3 presents the numerical results, highlighting halo diagnostics on ΔR and $\Delta M/M$, the luminous-versus-gravitational radius comparison on the M - R plane, and

the impact of a percent–level vacuum–like fraction. Section 4 summarizes the main findings, outlines multimessenger implications, and delineates modeling limitations and observational strategies for near-term tests.

2 Dark influence on the structure equations

We consider static, spherically symmetric NSs composed of ordinary (baryonic) matter and a unified dark sector, which includes DM and DE. The spacetime geometry is described by

$$ds^2 = e^{2\nu(r)} dt^2 - \frac{dr^2}{1 - 2m(r)/r} - r^2(d\theta^2 + \sin^2\theta d\phi^2), \quad (2.1)$$

where $m(r)$ is the enclosed gravitational mass. Each sector $i \in \{\text{bm}, \chi, \text{de}\}$ is modeled as a perfect fluid with energy–momentum tensor

$$T_{(i)}^{\mu\nu} = (\epsilon_i + p_i)u^\mu u^\nu - p_i g^{\mu\nu}, \quad (2.2)$$

and the total tensor is the explicit sum

$$T^{\mu\nu} = \sum_{i \in \{\text{bm}, \chi, \text{de}\}} T_{(i)}^{\mu\nu}. \quad (2.3)$$

To account for a potential non-gravitational coupling, we follow the unified Model III of Ref. [32] and allow the dark sector to exchange energy with baryons. This is described by a source term Q such that the total system remains covariantly conserved while the individual sectors are not:

$$T_{;\mu}^{\mu\nu} = 0, \quad T_{(\text{bm});\mu}^{\mu\nu} = Q, \quad T_{(\text{dark});\mu}^{\mu\nu} = -Q, \quad (2.4)$$

with $T_{(\text{dark})}^{\mu\nu} \equiv T_{(\chi)}^{\mu\nu} + T_{(\text{de})}^{\mu\nu}$. For the interaction term, we adopt the phenomenological form from [32],

$$Q \equiv \alpha \frac{d\epsilon_{\text{dark}}}{dr} = \alpha \frac{d\epsilon_{\text{dark}}}{dp_{\text{dark}}} \frac{dp_{\text{dark}}}{dr}, \quad (2.5)$$

where α is a dimensionless coupling (we set $\alpha = 1$ unless stated otherwise). By this convention, $Q > 0$ denotes an energy flow *into* the baryons, while $Q < 0$ represents energy flowing *out of* them.

Combining the field equations with the conservation laws in Eqs. (2.1)–(2.5) yields the modified system for hydrostatic structure:

$$\frac{dp_{\text{bm}}}{dr} + \frac{(p_{\text{bm}} + \epsilon_{\text{bm}})(m + 4\pi r^3 p)}{r^2 - 2mr} = Q, \quad (2.6)$$

$$\frac{dp_{\text{dark}}}{dr} + \frac{(p_{\chi} + \epsilon_{\chi})(m + 4\pi r^3 p)}{r^2 - 2mr} = -Q, \quad (2.7)$$

$$\frac{dm}{dr} = 4\pi r^2 \epsilon, \quad (2.8)$$

$$\frac{d\nu}{dr} = \frac{m + 4\pi r^3 p}{r^2 - 2mr}. \quad (2.9)$$

Here, $p = p_{\text{bm}} + p_{\text{dark}}$ and $\epsilon = \epsilon_{\text{bm}} + \epsilon_{\text{dark}}$ are the total pressure and energy density. Note that in the dark sector's hydrostatic equation (2.7), the active gravitational mass term ($\epsilon_{\text{dark}} + p_{\text{dark}}$) simplifies to $(\epsilon_{\chi} + p_{\chi})$. This is because the vacuum-like component satisfies $p_{\text{de}} = -\epsilon_{\text{de}}$, and thus its contribution vanishes. This system is solved subject to regularity conditions at the center, namely $m(0) = 0$ and finite pressures $p_i(0)$. The stellar surface R is located where the *total* pressure vanishes, $p(R) = 0$, which defines the total mass $M \equiv m(R)$. We also define the baryonic radius, R_{bm} , as the location where the pressure of the baryonic fluid vanishes, $p_{\text{bm}}(R_{\text{bm}}) = 0$. If the dark component's pressure extends beyond this point, becoming zero at a larger radius, the star is surrounded by a dark halo.

To close the hydrostatic system in Eqs. (2.6)–(2.9), we must specify the barotropic relations $p_i(\epsilon_i)$ for each constituent. We adopt the following equations of state:

- **Baryonic matter:** We model the cold, catalyzed baryonic component as charge-neutral, β -equilibrated $npe\mu$ matter. Its properties are described by the Akmal - Pandharipande - Ravenhall (APR) EOS [33], which is built from variational chain-summation calculations using realistic two- and three-nucleon forces (Argonne v_{18} + Urbana IX) with relativistic boost corrections. For computational purposes, we employ the Generalized Piecewise Polytopic (GPP) representation from Ref. [34], which approximates the microphysical APR curve with polytropic segments while ensuring continuity of pressure, energy density, and sound speed. This yields a thermodynamically consistent surrogate across all relevant densities. The outer layers are treated by matching this core EOS to a GPP fit of the unified SLy(4) crust model [35]. This implementation strategy for the baryonic EOS has been used in our recent work [32, 36].
- **Dark matter:** DM candidates span many orders of magnitude in mass and statistics, from ultralight bosons in the wave regime to multi-TeV particulate scenarios [37, 38]. From the standpoint of particle microphysics, a particularly well-motivated and widely used benchmark for the dark component inside NSs is fermionic DM modeled as a cold, degenerate Fermi fluid. This choice is conservative and phenomenologically robust: degeneracy pressure provides a minimal, model-agnostic source of support without invoking condensate physics or model-dependent self-interactions, and it encompasses a broad class of WIMP-like scenarios explored in the NS context [5, 18, 20, 21, 39]. We therefore adopt a single-species, spin-1/2 *non-interacting* Fermi gas at $T = 0$ as our baseline. In the non-interacting limit the EOS of the relativistic Fermi fluid is

$$p_{\chi} = \frac{m_{\chi}^4}{24\pi^2} \left\{ z \sqrt{z^2 + 1} (2z^2 - 3) + 3 \sinh^{-1}(z) \right\}, \quad (2.10)$$

$$\epsilon_{\chi} = \frac{m_{\chi}^4}{8\pi^2} \left\{ z \sqrt{z^2 + 1} (2z^2 + 1) - \sinh^{-1}(z) \right\}, \quad (2.11)$$

where m_{χ} is the fermion mass and $z \equiv k_{F\chi}/m_{\chi}$ is the dimensionless Fermi momentum (we use natural units $\hbar = c = 1$ and a spin degeneracy $g_{\chi} = 2$). The number density is $n_{\chi} = k_{F\chi}^3/(3\pi^2)$, and the chemical potential is $\mu_{\chi} = m_{\chi}\sqrt{1 + z^2}$. This ideal EOS provides a transparent baseline to quantify how the dark component affects stellar structure in our two-fluid calculations.

- **Dark energy:** We model the DE sector as a vacuum-like component with local EOS $p_{\text{de}} = -\epsilon_{\text{de}}$. This component carries a positive energy density and negative pressure that may vary with radius. In the stellar-structure equations, it contributes to the

mass profile through $4\pi r^2 \epsilon_{\text{de}}(r)$ and reduces effective pressure support in hydrostatic balance, thereby lowering the maximum mass [36].

To close the system, we must provide a prescription for setting the central boundary conditions that determine the relative abundances of each component. We achieve this by parameterizing the central energy densities. First, we fix the total central energy density, $\epsilon_c \equiv \epsilon(r=0)$. Then, we introduce two dimensionless parameters, y_{bm} and x_χ , which govern the partition of this energy density.

The parameter $y_{\text{bm}} \in [0, 1]$ sets the fraction of the total central density corresponding to baryonic matter:

$$\epsilon_{\text{bm}}(0) = y_{\text{bm}} \epsilon_c, \quad (2.12)$$

$$\epsilon_{\text{dark}}(0) = (1 - y_{\text{bm}}) \epsilon_c. \quad (2.13)$$

The limiting case $y_{\text{bm}} = 1$ yields a purely baryonic center, whereas $y_{\text{bm}} = 0$ describes a center composed entirely of dark components. Equivalently, we define the central dark-sector fraction as $y_{\text{dark}} \equiv 1 - y_{\text{bm}}$.

Next, the parameter $x_\chi \in [0, 1]$ specifies the internal composition of the dark sector at $r = 0$:

$$\epsilon_\chi(0) = x_\chi \epsilon_{\text{dark}}(0), \quad (2.14)$$

$$\epsilon_{\text{de}}(0) = (1 - x_\chi) \epsilon_{\text{dark}}(0). \quad (2.15)$$

Here, $x_\chi = 1$ signifies a dark sector made entirely of dark matter, whereas $x_\chi = 0$ corresponds to a pure dark-energy component.

With the central conditions fully specified by the set $\{\epsilon_c, y_{\text{bm}}, x_\chi\}$, we numerically integrate the structure equations (2.6)–(2.8) from the center ($r = 0$) to the stellar surface ($r = R$), defined by the vanishing of the total pressure, $p(R) = 0$. This procedure allows us to construct the mass–radius relations and investigate the impact of the dark sector’s composition and interactions on the global properties of the NS.

3 Results

3.1 Halo diagnostics from radius and mass excess

Figure 1 quantifies the structural impact of the dark sector by plotting two key diagnostics against the total gravitational mass M : the absolute radius excess, $\Delta R \equiv R - R_{\text{bm}}$, and the fractional mass excess, $\Delta M/M \equiv (M - M_{\text{bm}})/M$. Here, R_{bm} and M_{bm} represent the radius and mass of the baryonic component, which are in principle accessible via electromagnetic observations, whereas R and M are the total values that determine the exterior spacetime and gravitational response. The figure compares sequences for two fermionic dark matter masses ($m_\chi = 400$ MeV and 1 GeV), two central baryonic fractions ($1 - y_{\text{dark}}$, corresponding to $y_{\text{bm}} = 0.982$ and 0.965), and two central dark-sector compositions: a pure dark matter fluid ($x_\chi = 1.0$) and a unified fluid with a 3% vacuum-energy component ($x_\chi = 0.97$). Three distinct physical trends emerge from these comparisons.

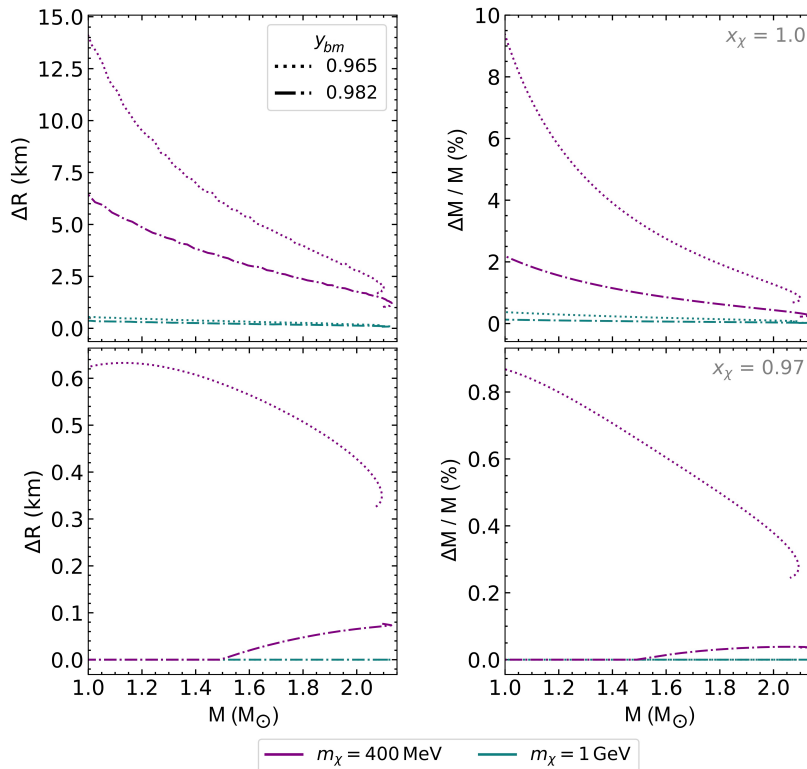


Figure 1. Radius excess $\Delta R \equiv R - R_{\text{bm}}$ (top) and fractional mass excess $\Delta M/M \equiv (M - M_{\text{bm}})/M$ (bottom) as functions of the gravitational mass M for dark-matter-admixed NSs with an interacting dark sector. Here R and M are the total (gravitational) radius and mass that source the exterior spacetime, while R_{bm} and M_{bm} are the baryonic (electromagnetic) counterparts inferred from the luminous component. Curves compare fermionic dark-matter masses $m_\chi = 1$ GeV and 400 MeV, two central baryon fractions $y_{\text{bm}} = \{0.982, 0.965\}$, and internal dark-sector partitions $x_\chi = \{1.0, 0.97\}$ (the latter corresponding to a 3% vacuum-like fraction when $x_\chi = 0.97$). Lighter m_χ and smaller y_{bm} produce extended halos that substantially increase R , while the associated change in M is present but comparatively modest; introducing a small vacuum-like admixture ($x_\chi < 1$) leads to a marked reduction in the halo’s radial extent and mass.

Dependence on Dark Matter Particle Mass. The most prominent trend is the strong dependence of halo formation on the DM particle mass, m_χ . For a fixed central composition, configurations with lighter DM particles ($m_\chi = 400$ MeV) develop substantially more extended halos (larger ΔR) and greater mass excesses ($\Delta M/M$) than their counterparts with heavier particles ($m_\chi = 1$ GeV). This behavior follows directly from the cold, degenerate Fermi-gas scaling: at fixed number density n_χ , the pressure obeys $p_\chi \propto n_\chi^{5/3} m_\chi^{-1}$ in the nonrelativistic regime, so lighter fermions provide more pressure per unit energy density and can support a diffuse, pressure-held envelope beyond the baryonic surface, inflating R while only mildly increasing M .

This mass ordering corroborates the canonical picture established in previous work. Two-fluid studies consistently show that sub-GeV fermions favor extended halos and large radius shifts at fixed mass, whereas $\mathcal{O}(\text{GeV})$ fermions tend to suppress halo formation—driving $R \rightarrow R_{\text{bm}}$ and yielding small $R - R_{\text{bm}}$ —rather than producing robust dark cores; core-like configurations arise only in specific setups and/or at sufficiently large dark fractions (see,

e.g., [20]), while analyses focused on light/admixed DM typically find halo-dominated or halo-absent regimes, not stable DM cores [18, 19, 22]. At the opposite extreme, very heavy (\gtrsim GeV) DM components soften the effective EoS without forming halos, lowering M_{\max} and potentially conflicting with the $2 M_{\odot}$ bound—consistent with early effective-fluid treatments [21]. The observational ramifications of halo formation are likewise well documented: tidal-response calculations identify large changes in Love numbers and deformabilities when a low-density dark envelope is present [18, 19], and pulse-profile (self-lensing) studies show that the footprint scales with the “halo compactness” rather than with halo mass alone [23–25]. These precedents motivate the mass scan adopted here: $m_{\chi} = 400$ MeV as a representative halo-forming benchmark and $m_{\chi} = 1$ GeV as a baseline where halos are strongly quenched.

Dependence on Dark Matter Abundance. The overall scale of the dark halo is, as expected, controlled by the dark abundance, here parameterized by the central dark fraction y_{dark} (equivalently, by the global mass fraction $f_{\chi} \equiv M_{\chi}/M$ along a sequence). Decreasing the central baryonic content (i.e., lowering y_{bm} from 0.982 to 0.965) systematically increases both ΔR and $\Delta M/M$ for all models. A larger reservoir of DM allows a greater portion of the dark fluid to settle into low-density hydrostatic equilibrium outside the luminous surface, so the gravitational radius R grows while the stellar mass M shifts more modestly. This *radius-dominant* response with increasing f_{χ} is the same qualitative behavior reported in two-fluid calculations: for fixed m_{χ} , raising the dark fraction enlarges the R – R_{bm} split and enhances tidal effects when halos form [18, 19]. Quantitatively, Ref. [20] mapped the (m_{χ}, f_{χ}) plane with a realistic nuclear EoS and identified a *critical* curve $f_{\chi}^{\text{crit}}(m_{\chi})$ from the $2 M_{\odot}$ condition, showing that (i) sub-GeV masses tolerate sizable f_{χ} (halo regimes) while (ii) $\mathcal{O}(\text{GeV})$ masses require small f_{χ} to avoid suppressing M_{\max} below $2 M_{\odot}$ (halo-quenched regimes). In bosonic-DM studies with repulsive self-interactions, the same monotonicity with abundance appears—larger fractions amplify radius shifts and tidal imprints up to observational bounds on $\Lambda_{1.4}$ —thereby restricting f_{χ} to percent-level values [22]. Early effective-fluid analyses already noted that increasing the dark admixture softens the global EoS and lowers M_{\max} , tightening the viable range of f_{χ} when m_{χ} is heavy [21]. On the observational side, both tidal-deformability studies and pulse-profile/self-lensing analyses emphasize that the *detectability* of a given f_{χ} depends on how much of it resides in the outer, low-density layer: halo-dominated configurations at moderate f_{χ} can produce large changes in k_2 and Λ [18, 19] and measurable flux-peak modulations set by halo compactness rather than by f_{χ} alone [23–25]. Our trends for $m_{\chi} = 400$ MeV (large ΔR at lower y_{bm}) and for $m_{\chi} = 1$ GeV (halo suppression even as y_{bm} decreases) therefore reproduce the established abundance systematics and provide a controlled baseline to assess how adding a vacuum-like fraction further quenches the halo at fixed f_{χ} .

Effect of a Dark Energy Admixture. A central novelty of this work is the explicit inclusion of a vacuum-like component in the unified dark sector and the demonstration—in *the halo-forming mass regime*—that even a $\sim 3\%$ dark-energy (DE) fraction ($x_{\chi} = 0.97$) efficiently *quenches halo formation*. As seen in Figure 1, the DE admixture drives a sharp contraction of the exterior dark layer: for the same central partition and fermion mass, the radius excess decreases from $\mathcal{O}(10)$ km (pure DM) to sub-kilometer levels, while the fractional mass excess is suppressed from several percent (up to $\sim 10\%$) to the sub-percent regime—i.e., order-of-magnitude reductions in $\Delta M/M$ and factors $\gtrsim 10$ – 20 in ΔR , with the effect most pronounced for $m_{\chi} = 400$ MeV and still visible at 1 GeV. Physically, this behavior follows

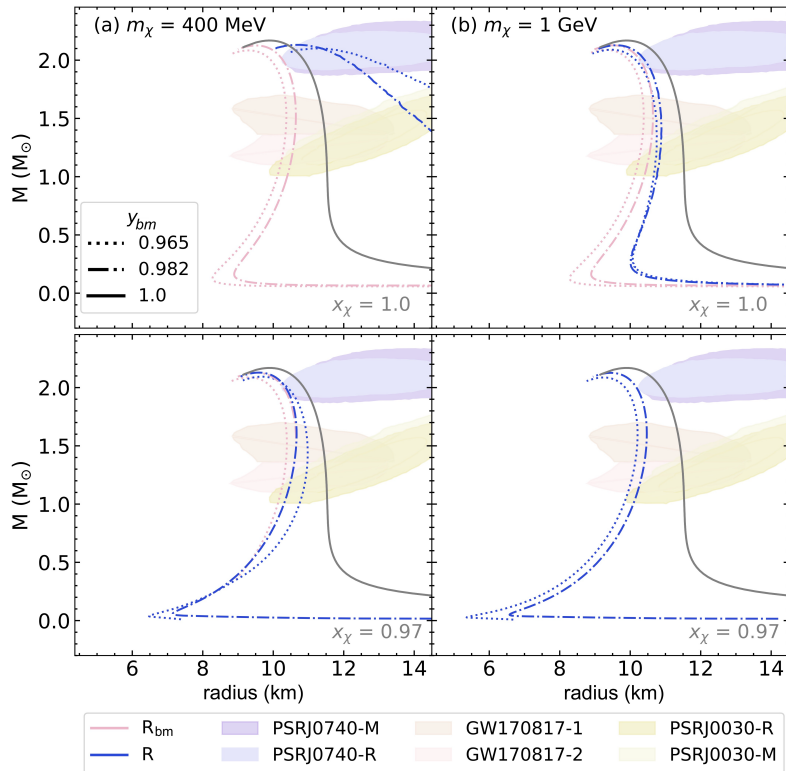


Figure 2. Mass–radius relations of NSs modified by dark sector interactions, constrained by observations (background clouds). Two primary markers are presented: pink curves, representing the contribution from the luminous radius alone, and blue curves, indicating the total gravitational radius of the objects. The solid gray curve denotes the baseline case in which only baryonic matter is considered ($y_m = 1.0$).

directly from the structure equations in our Model III: the vacuum sector contributes negative pressure but *no* inertial term in the TOV force balance, since $\epsilon_{\text{de}} + p_{\text{de}} = 0$; as a result, at fixed ϵ_{dark} the supporting pressure comes almost solely from the fermionic DM, which is now a smaller fraction of the dark sector. The net effect is a steeper outward decline of the *total* pressure and an earlier satisfaction of the surface condition $p(R) = 0$, which collapses the halo and drives $R \rightarrow R_{\text{bm}}$. In addition, while ϵ_{de} still feeds the mass function $m(r)$, the lack of a corresponding pressure–support term enhances the gravity–to–support imbalance in the outer layers, reinforcing the halo quenching.

This DE–induced suppression is *qualitatively new* relative to previous dark matter admixed NSs (DANS) studies—which either neglected DE entirely and focused on pure DM (fermionic or bosonic) [18–20, 22, 23, 25] or, in the case of our previous work [31], explored DE at $m_\chi = 10$ GeV where halos do not form. Those works established that sub–GeV fermions favor extended halos and large radius shifts at fixed mass, whereas $\mathcal{O}(\text{GeV})$ masses tend to *suppress* halos; our results extend that picture by showing that a *percent–level* DE fraction can suppress halos *even within* an otherwise halo–friendly mass range, thereby collapsing $R - R_{\text{bm}}$ while leaving M comparatively unchanged.

3.2 Mass–radius relations with luminous vs gravitational radii

Figure 2 recasts the diagnostics of Figure 1 in the M – R plane, showing, for each sequence, both the baryonic radius R_{bm} and the total radius R . The microphysical setups are identical to those in Figure 1— $m_\chi = 400$ MeV and 1 GeV, $x_\chi = 1.0$ and 0.97, and $y_{\text{bm}} \in \{0.982, 0.965\}$ —with the sole addition of a purely baryonic baseline, $y_{\text{bm}} = 1$, used here as an on-plot benchmark. In this representation, the radius excess $\Delta R \equiv R - R_{\text{bm}}$ appears as a horizontal offset between paired curves: whenever a low-density dark envelope forms, R lies to the right of R_{bm} . For $m_\chi = 400$ MeV, extended regions with R significantly larger than R_{bm} emerge, whereas for $m_\chi = 1$ GeV the differences are smaller but still appreciable (upper panels). Introducing a percent-level vacuum-like fraction ($x_\chi = 0.97$) largely collapses that separation and drives $R \rightarrow R_{\text{bm}}$ (lower panels). It is evident that the radius response dominates over the mass response: the locus of maximum mass and the overall M scale shift only modestly compared with the horizontal displacement in R as the dark-sector parameters vary.

We overlay NICER inferences (PSR J0030+0451 and PSR J0740+6620) and GW constraints from GW170817 (LIGO/Virgo) [26–30]. Since $\Delta M/M$ is typically sub-percent in the regimes probed here, we display the total gravitational mass M for all tracks. Crucially, the two classes of measurements constrain different radii: NICER hotspot modeling refers to the photospheric surface and should be compared against the M – R_{bm} tracks, whereas tidal deformability from binary inspirals probes the exterior spacetime and thus constrains the M – R tracks. Observationally, the GW170817 credible region lies slightly to the left (smaller R) of the NICER posteriors—a model-independent ordering. By contrast, halo formation generically predicts $R > R_{\text{bm}}$ at fixed M , which would place the GW-traced M – R locus to the right of the NICER-traced M – R_{bm} locus. The fact that we observe the opposite implies that any halo, if present, must be thin, with $\Delta R \lesssim 2$ –3 km—a scale set by the width of the radial interval where the NICER posteriors and the GW170817 credible region overlap in the M – R plane (i.e., the common radius band permitted by both). Such suppression arises naturally if the dark-matter particle mass lies near the upper end of the sub-GeV range and/or if a percent-level vacuum-like fraction is present, which reduces ΔR .

4 Summary and conclusions

We have investigated NSs hosting a unified dark sector composed of cold, degenerate fermionic DM and a vacuum-like DE component. Our analysis employed a general-relativistic two-fluid hydrostatic framework that allows for a covariantly conserved, gradient-driven energy exchange between baryons and the dark sector. The study focuses on the *halo-forming* mass range for fermionic DM, $m_\chi = \{400 \text{ MeV}, 1 \text{ GeV}\}$, and on observables that disentangle luminous from gravitational structure, namely the radius and mass excesses $\Delta R \equiv R - R_{\text{bm}}$ and $\Delta M/M \equiv (M - M_{\text{bm}})/M$.

A first outcome of this study is the confirmation of well-established systematics regarding the roles of the DM particle mass and its abundance. Using the same diagnostics across sequences, we find that sub-GeV fermions (e.g., $m_\chi = 400$ MeV) give rise to extended, low-density halos that increase the gravitational radius R by several kilometers, while the accompanying change in mass remains comparatively modest. By contrast, near-GeV masses (e.g., $m_\chi = 1$ GeV) markedly reduce halo extent and bring R closer to R_{bm} at comparable M . The abundance trend is likewise clear: for fixed m_χ , decreasing the central baryon frac-

tion y_{bm} amplifies both the radius and mass excesses. These behaviors are consistent with two-fluid calculations of fermionic DANS and with related bosonic-DM analyses [18–22].

A central result of this study concerns the effect of a percent-level vacuumlike fraction in the unified dark sector. In our sequences, introducing a small DE admixture (e.g., $x_\chi = 0.97$, corresponding to a 3% DE fraction) markedly reduces halo extent and mass even in otherwise halo-friendly regimes: ΔR drops from several kilometers to sub-kilometer scales, while $\Delta M/M$ is suppressed from a few percent to the sub-percent level. The effect is most pronounced for $m_\chi = 400$ MeV and remains visible at 1 GeV. The mechanism is hydrostatic and follows directly from the structure equations: the vacuum component contributes negative pressure to the TOV balance, so the total pressure support in the outer layers decreases while $m(r)$ still receives a contribution from ϵ_{de} . This enhances the outward decline of the total pressure, reducing the radius at which $p(R) = 0$ and driving R closer to R_{bm} , with a comparatively smaller impact on M . To our knowledge, no prior DANS analysis has reported and quantitatively characterized percent-level DE-induced halo contraction in the halo-forming regime.

These results have immediate multimessenger implications. Because gravitational waves probe R , while X-ray pulse-profile modeling constrains a photospheric radius tied to R_{bm} , halo-forming configurations naturally predict a split between the radii inferred by the different channels. In fact, halo-bearing models generically predict $R > R_{\text{bm}}$ at fixed M , which would place the GW-inferred M - R locus to the *right* of the X-ray-inferred M - R_{bm} locus. Current data show the opposite ordering: the credible region from GW170817 lies slightly to the *left* (smaller radii) of the NICER posteriors, strongly disfavoring large halos and implying a tight bound $\Delta R \equiv R - R_{\text{bm}} \lesssim 2$ –3 km. Within our framework this small offset is naturally achieved not only for fermionic DM with masses near the GeV scale, but also for lighter DM provided a percent-level vacuum-like fraction is present, both cases shrinking the dark envelope while leaving M comparatively less affected.

Acknowledgments

LFA was supported by the Brazilian agency Coordenação de Aperfeiçoamento de Pessoal de Nível Superior (CAPES). GL LFA acknowledges support from the Brazilian agency Coordenação de Aperfeiçoamento de Pessoal de Nível Superior (CAPES). GL acknowledges partial financial support from the Brazilian agency CNPq (Grant No. 316844/2021-7). JASL is partially supported by the Brazilian agencies CNPq (Grant No. 310038/2019-7), CAPES (Grant No. 88881.068485/2014), and FAPESP (LLAMA Project No. 11/51676-9).

References

- [1] G. Bertone, D. Hooper and J. Silk, *Particle dark matter: Evidence, candidates and constraints*, *Phys. Rept.* **405** (2005) 279 [[hep-ph/0404175](#)].
- [2] M. Schumann, *Direct detection of wimp dark matter: Concepts and status*, *J. Phys. G* **46** (2019) 103003 [[1903.03026](#)].
- [3] G. Bertone and T.M. Tait, *A new era in the search for dark matter*, *Nature* **562** (2018) 51 [[1810.01668](#)].
- [4] T. Güver, A.E. Erkoca, M.H. Reno and I. Sarcevic, *On the capture of dark matter by neutron stars*, *JCAP* **05** (2014) 013 [[1201.2400](#)].

- [5] I. Goldman and S. Nussinov, *Weakly interacting massive particles and neutron stars*, *Phys. Rev. D* **40** (1989) 3221.
- [6] C. Kouvaris, *Wimp annihilation and cooling of neutron stars*, *Phys. Rev. D* **77** (2008) 023006 [0708.2362].
- [7] N.F. Bell, G. Busoni, S. Robles and M. Virgato, *Thermalization and annihilation of dark matter in neutron stars*, *JCAP* **01** (2024) 006 [2312.11892].
- [8] J. Bramante and N. Raj, *Dark matter in compact stars*, *Phys. Rept.* **1052** (2024) 1 [2308.12301].
- [9] G. Baym, D. Beck, P. Geltenbort and J. Shelton, *Testing dark decays of baryons in neutron stars*, *Phys. Rev. Lett.* **121** (2018) 061801 [1802.08282].
- [10] M. Hippert, E. Dillingham, H. Tan, D. Curtin, J. Noronha-Hostler and N. Yunes, *Dark matter or regular matter in neutron stars? how to tell the difference from the coalescence of compact objects*, *Phys. Rev. D* **107** (2023) 115028 [2211.14364].
- [11] R.K. Leane, K.C.Y. Ng and J.F. Beacom, *Powerful Solar Signatures of Long-Lived Dark Mediators*, *Phys. Rev. D* **95** (2017) 123016 [1703.04629].
- [12] J.F. Acevedo, J. Bramante, Q. Liu and N. Tyagi, *Neutrino and gamma-ray signatures of inelastic dark matter annihilating outside neutron stars*, *JCAP* **03** (2025) 028 [2404.10039].
- [13] B. Dasgupta, A. Gupta and A. Ray, *Dark matter capture in celestial objects: light mediators, self-interactions, and complementarity with direct detection*, *JCAP* **10** (2020) 023 [2006.10773].
- [14] S. Shirke, B. Pradhan, D. Chatterjee, L. Sagunski and J. Schaffner-Bielich, *Effects of dark matter on f -mode oscillations of neutron stars*, *Phys. Rev. D* **110** (2024) 063025 [2403.05652].
- [15] S.-C. Leung, M.-C. Chu and L.-M. Lin, *Dark-matter admixed neutron stars*, *Phys. Rev. D* **84** (2011) 107301 [1111.1787].
- [16] G. Panotopoulos and I. Lopes, *Dark matter effect on realistic equation of state in neutron stars*, *Phys. Rev. D* **96** (2017) 083004 [1709.06312].
- [17] J. Ellis, G. Hütsi, K. Kannike, L. Marzola, M. Raidal and V. Vaskonen, *Dark matter effects on neutron star properties*, *Phys. Rev. D* **97** (2018) 123007 [1804.01418].
- [18] K.-L. Leung, M.-c. Chu and L.-M. Lin, *Tidal deformability of dark matter admixed neutron stars*, *Phys. Rev. D* **105** (2022) 123010 [2207.02433].
- [19] A. Nelson, S. Reddy and D. Zhou, *Dark halos around neutron stars and gravitational waves*, *JCAP* **07** (2019) 012 [1803.03266].
- [20] D. Scordino and I. Bombaci, *Dark matter admixed neutron stars with a realistic nuclear equation of state from chiral nuclear interactions*, *JHEAp* **45** (2025) 371 [2405.19251].
- [21] A. Li, F. Huang and R.-X. Xu, *Too massive neutron stars: The role of dark matter?*, *Astropart. Phys.* **37** (2012) 70 [1208.3722].
- [22] D.R. Karkevandi, S. Shakeri, V. Sagun and O. Ivanytskyi, *Bosonic dark matter in neutron stars and its effect on gravitational wave signal*, *Phys. Rev. D* **105** (2022) 023001 [2109.03801].
- [23] S. Shawqi and S.M. Morsink, *Interpreting Mass and Radius Measurements of Neutron Stars with Dark Matter Halos*, *Astrophys. J.* **975** (2024) 123 [2406.03332].
- [24] Y. Liu, H.-B. Li, Y. Gao, L. Shao and Z. Hu, *Effects from dark matter halos on x-ray pulsar pulse profiles*, *Phys. Rev. D* **110** (2024) 083018 [2408.04425].
- [25] Z. Miao, Y. Zhu, A. Li and F. Huang, *Dark Matter Admixed Neutron Star Properties in the Light of X-Ray Pulse Profile Observations*, *Astrophys. J.* **936** (2022) 69 [2204.05560].
- [26] LIGO SCIENTIFIC, VIRGO collaboration, *GW170817: Measurements of neutron star radii and equation of state*, *Phys. Rev. Lett.* **121** (2018) 161101 [1805.11581].

- [27] M.C. Miller et al., *The Radius of PSR J0740+6620 from NICER and XMM-Newton Data*, *Astrophys. J. Lett.* **918** (2021) L28 [2105.06979].
- [28] M. Miller et al., *PSR J0030+0451 Mass and Radius from NICER Data and Implications for the Properties of Neutron Star Matter*, *Astrophys. J. Lett.* **887** (2019) L24 [1912.05705].
- [29] T.E. Riley et al., *A NICER View of the Massive Pulsar PSR J0740+6620 Informed by Radio Timing and XMM-Newton Spectroscopy*, *Astrophys. J. Lett.* **918** (2021) L27 [2105.06980].
- [30] T.E. Riley et al., *A NICER View of PSR J0030+0451: Millisecond Pulsar Parameter Estimation*, *Astrophys. J. Lett.* **887** (2019) L21 [1912.05702].
- [31] L.F. Araujo, G. Lugones and J.A.S. Lima, *Dark interactions in neutron star interiors: The interplay of baryons, dark matter, and dark energy*, *Phys. Rev. D* **112** (2025) 083012 [2509.16484].
- [32] L.F. Araújo, G. Lugones and J.A.S. Lima, *Dark interactions in neutron star interiors: the interplay of baryons, dark matter, and dark energy*, Submitted to publication (2025) .
- [33] A. Akmal, V.R. Pandharipande and D.G. Ravenhall, *The Equation of state of nucleon matter and neutron star structure*, *Phys. Rev. C* **58** (1998) 1804 [nucl-th/9804027].
- [34] M.F. O’Boyle, C. Markakis, N. Stergioulas and J.S. Read, *Parametrized equation of state for neutron star matter with continuous sound speed*, *Physical Review D* **102** (2020) 083027.
- [35] F. Douchin and P. Haensel, *A unified equation of state of dense matter and neutron star structure*, *Astron. Astrophys.* **380** (2001) 151 [astro-ph/0111092].
- [36] L.F. Araujo, J.A.S. Lima and G. Lugones, *Impact of dark energy on the structure of neutron stars: The vacuum case*, *Phys. Rev. D* **110** (2024) 043040 [2408.01006].
- [37] L. Hui, J.P. Ostriker, S. Tremaine and E. Witten, *Ultralight scalars as cosmological dark matter*, *Phys. Rev. D* **95** (2017) 043541 [1610.08297].
- [38] D.J.E. Marsh, *Axion cosmology*, *Phys. Rept.* **643** (2016) 1 [1510.07633].
- [39] C. Kouvaris and P. Tinyakov, *Constraining Asymmetric Dark Matter through observations of compact stars*, *Phys. Rev. D* **83** (2011) 083512 [1012.2039].